

Optimal High-Resolution Adaptive Sampling of Deterministic Signals

Yehuda Dar and Alfred M. Bruckstein

Abstract—In this work we study the topic of high-resolution adaptive sampling of a given deterministic signal and establish a connection to classic approaches to high-rate quantization. Specifically, we formulate solutions to the task of optimal high-resolution sampling, counterparts of well-known results for high-rate quantization. Our results reveal that the optimal high-resolution sampling structure is determined by the density of the signal-gradient energy, just as the probability-density-function defines the optimal high-rate quantization form. This paper has three main contributions: the first is establishing a fundamental paradigm bridging the topics of sampling and quantization. The second is a theoretical analysis of sampling, for arbitrary signal-dimension, relevant to the emerging field of high-resolution signal processing. The third is a new approach to nonuniform sampling of one-dimensional signals that is experimentally shown to outperform an optimized tree-structured sampling technique.

Index Terms—High-resolution sampling, adaptive sampling, high-rate quantization.

I. INTRODUCTION

SAMPLING and quantization are fundamental processes in signal digitization and coding techniques. Each of them is a field of research rich in theoretical and practical studies. Quantization addresses the problem of discretizing a range of values by a mapping function, usually based on decomposition of the range into a finite set of non-intersecting regions. Sampling a given deterministic signal, defined over a continuous and bounded domain, is the task of discretizing the signal representation (for example, representing a finite-length one-dimensional signal as a vector). In this paper we consider nonuniform sampling that relies on segmentation of the signal domain into non-overlapping regions, each represented by a single scalar coefficient (we do not consider here generalized sampling that uses projections of the signal onto a discrete set of orthonormal functions).

The discretizations in quantization and sampling were first implemented in their simplest forms relying on uniform divisions of the respective domains. Then, the quantizer designs progressed to utilize nonuniform structures, exploiting input-data statistics to improve rate-distortion performance. In his fundamental work, Bennett [1] suggested to implement nonuniform scalar quantization based on a companding model – where the input value goes through a nonlinear mapping (compressor), the obtained value being uniformly quantized and then mapped back via the inverse of the nonlinearity (expander). Moreover, under high-rate assumptions, Bennett derived a formula for approximating the quantizer distortion based on the source probability-density-function and

the derivative of the nonlinear compressor function. This important formula is often referred to as Bennett’s integral. Bennett’s work was followed by a long line of theoretic and algorithmic studies of the nonuniform quantization problem. A prominent branch of research addressed the scenario of nonuniform quantization at high-rates (for example, see [2], [3]), where the quantizer has a large number of representation-values to be wisely located at the quantizer-design stage. The popularity of high-rate studies is due not only to their relevance in addressing high-quality coding applications, but also to the possibility to gain useful theoretical perspectives. Specifically, reasonable assumptions made for high-rate quantization often led to convenient closed-form mathematical solutions that, in turn, provided deep insights into rate-distortion trade-offs.

Practical signal-compression usually addresses a digital high-resolution input function that is going through a nonuniform adaptive partitioning of the domain followed by a quantization procedure that suits the partition size and shape. Analytically, the digital input can be regarded as a signal defined over a continuous-domain that needs to be nonuniformly sampled and quantized. In practical coding procedures, the nonuniform domain segmentation relies on structured formations in order to reduce the bit-cost and computational complexity (examples for the common use of tree-structured partitioning are available in [4], [5]). This application is one of the main motivations to the study of adaptive sampling of deterministic signals. Nevertheless, we consider here the nonuniform sampling problem in its most general form in order to provide insights to the basic sampling problem, that may be useful to problems beyond compression. For example, adaptive sampling is often used in computer-graphics in the task of Halftoning (e.g., [6], [7]) and in rendering an image from a 2D/3D-graphical model, where the nonuniform sampling pattern is described by a point distribution (e.g., [8]–[12]). It should be noted that the signal-processing and computer-graphics contexts of the sampling problem are quite different. Interestingly, it was suggested in [10] to practically employ the Lloyd algorithm [13], originally intended for quantizer design, for improving the sampling point distribution. Recent studies [11], [12] extended the point-distribution computation to rely on kernel functions, such that the resulting task resembles a generalized signal-sampling procedure. While the conceptual relation between vector-quantization and data-representation has been practically utilized to some extent in graphics applications, we argue that a clear mathematical analysis that demonstrates the connection between quantization and high-resolution signal-sampling has not been provided yet.

In this paper we theoretically explore the task of high-resolution adaptive sampling of a given deterministic sig-

The authors are with the Department of Computer Science, Technion, Israel. E-mail addresses: {ydar, freddy}@cs.technion.ac.il.

nal. The sampling-analysis provided emerges from well-established guidelines applied in studies of high-rate quantization, hence, connecting sampling and quantization in a new and enlightening way. We analytically formulate the optimal high-resolution sampling of one-dimensional signals, based on the Mean-Squared-Error (MSE) criterion, showing that the optimal partitioning is determined by the cube-root of the signal-derivative energy. This result corresponds to the work by Panter and Dite [2], where the optimal one-dimensional quantizer is designed based on the cube-root of the probability-density-function. We also connect this result to the fundamental analysis given by Bennett [1] for high-rate nonuniform quantization based on companding. We continue our analysis by addressing the problem of sampling K -dimensional signals. We show that the optimal sampling-point density is determined by the density of the $\frac{K}{K+2}$ -power of the signal-gradient energy, a generalization of the one-dimensional result. We obtain this result based on assumptions that parallel a famous conjecture given by Gersho [3] in his analysis of high-rate quantization.

Gersho's conjecture states that, for asymptotically high rate, the optimal K -dimensional quantizer is formed by regions that are approximately congruent and scaled versions of a K -dimensional convex polytope that optimally tessellates the K -dimensional space (where the polytope optimality is in the sense of minimum normalized moment of inertia [3]). The latter holds for a given K only if the optimal tessellation of the K -dimensional space is a lattice, and therefore constructed based on a single optimal polytope. This assumption significantly simplifies the explicit calculation of the quantizer's distortion. This conjecture draws its credibility from two prominent sources. First, it is known that the best tessellation is a lattice for $K = 1$ (based on equal-sized intervals) and for $K = 2$ (based on the hexagon shape [14]). While not proven yet for $K = 3$, it is also believed that the optimal three-dimensional tessellation is the body-centered cubic lattice [15], [16]. Second, Gersho's distortion formula conforms to the structure of the expression rigorously obtained by Zador [17]. Moreover, Gersho's conjecture determines the value of the multiplicative-constant (left unspecified) in Zador's formula. Hence, the possible inaccuracy in Gersho's conjecture will affect only the multiplicative constant, and the deviation is assumed to be moderate [18]. Due to this, the conjecture, still unproved for $K \geq 3$, is widely considered as a valuable tool for analysis of high-rate quantization (see the thorough discussion in [18]).

The analysis provided in this paper to high-resolution multidimensional sampling is based on two main assumptions. First, the signal is assumed to be approximately linear within each of the sampling regions. Second, sampling regions are assumed to be approximately congruent and scaled forms of the optimal K -dimensional tessellating convex polytope – just as in Gersho's conjecture for high-rate quantization. These high-resolution assumptions yield our main result that the optimal sampling-point density is determined by the density of the $\frac{K}{K+2}$ -power of the signal-gradient energy. We emphasize the importance of the signal's local-linearity assumption as a prerequisite stage that mathematically connects the signal-sampling problem to the conjecture on the high-resolution cell

arrangement.

This paper is organized as follows. In section II we mathematically analyze the optimal sampling of one-dimensional signals. In section III we provide an experimental evaluation of the proposed sampling method for one-dimensional signals. In section IV we generalize our study by theoretically addressing the optimal sampling of multidimensional signals. Section V concludes this paper.

II. ANALYSIS FOR ONE-DIMENSIONAL SIGNALS

A. Optimal High-Resolution Sampling

Let us consider a one-dimensional signal $\varphi(t)$ defined as the mapping

$$\varphi : [0, 1] \rightarrow [\varphi_L, \varphi_H], \quad (1)$$

i.e., it is defined for any t in the continuous interval $[0, 1]$ and having values from a continuous and bounded range $[\varphi_L, \varphi_H]$. This signal is sampled based on its partition to $N \in \mathbb{N}$ non-overlapping variable-length segments, where the i^{th} sub-interval $[a_{i-1}, a_i)$ is associated with the sample φ_i for $i = 1, \dots, N$. We assume a segmentation structure satisfying $a_0 = 0$, $a_N = 1$, and $a_{i-1} < a_i$ for $i = 1, \dots, N$. The sampling procedure is coupled with a reconstruction that provides the continuous-time piecewise-constant signal

$$\hat{\varphi}(t) = \varphi_i \quad \text{for } t \in [a_{i-1}, a_i). \quad (2)$$

The sampling is optimized to minimize the mean-squared-error (MSE), expressed as

$$MSE \left(\{a_i\}_{i=1}^{N-1}, \{\varphi_i\}_{i=1}^N \right) = \sum_{i=1}^N \int_{a_{i-1}}^{a_i} (\varphi(t) - \varphi_i)^2 dt \quad (3)$$

exhibiting the roles of the signal partitioning and sample values. Note that in (3), as also in this entire section, averaging over the unit-interval length is implicit.

Optimizing the sampling coefficients, $\{\varphi_i\}_{i=1}^N$, given a partitioning $\{a_i\}_{i=0}^N$ is a convex problem that can be analytically solved to show that the optimal i^{th} sampling-coefficient is the signal average over the corresponding subinterval, namely,

$$\varphi_i^{\text{opt}} = \frac{1}{\Delta_i} \int_{a_{i-1}}^{a_i} \varphi(t) dt \quad (4)$$

where $\Delta_i \triangleq a_i - a_{i-1}$ is the length of the i^{th} subinterval.

We continue the analysis by assuming high-rate sampling, meaning that N is large enough to result in small sampling-intervals that, however, may still have different lengths. Furthermore, the sampling intervals are assumed to be sufficiently small such that, within each of them, the signal is well approximated via a local linear form, i.e., for $t \in [a_{i-1}, a_i)$ ($i = 1, \dots, N$) the signal is

$$\varphi(t) \approx \beta_i t + \gamma_i. \quad (5)$$

The parameters β_i and γ_i can be determined by the first-order Taylor approximation of the signal around the center of the i^{th} sampling interval,

$$\varphi(t) \approx \varphi(t_i) + \varphi'(t_i) \cdot (t - t_i) \quad (6)$$

where $t_i \triangleq \frac{1}{2}(a_{i-1} + a_i)$ is the center of the i^{th} subinterval. Accordingly, the linearization parameters are set to $\beta_i = \varphi'(t_i)$ and $\gamma_i = \varphi(t_i) - \varphi'(t_i)t_i$.

Using the linear approximations, the "optimal" sampling coefficient of the i^{th} subinterval is

$$\varphi_i^{opt} \approx \frac{1}{\Delta_i} \int_{a_{i-1}}^{a_i} (\beta_i t + \gamma_i) dt = \beta_i t_i + \gamma_i \approx \varphi(t_i) \quad (7)$$

and this due to the fact that the average of a linear function over an interval is its value in the interval's center. Then, the MSE of the i^{th} subinterval is expressed as

$$\begin{aligned} MSE_i(a_{i-1}, a_i) &= \frac{1}{\Delta_i} \int_{a_{i-1}}^{a_i} (\varphi(t) - \varphi_i^{opt})^2 dt \quad (8) \\ &\approx \frac{1}{\Delta_i} \int_{a_{i-1}}^{a_i} [\beta_i t + \gamma_i - (\beta_i t_i + \gamma_i)]^2 dt \\ &= \frac{\beta_i^2}{\Delta_i} \int_{-\frac{\Delta_i}{2}}^{\frac{\Delta_i}{2}} \tilde{t}^2 d\tilde{t} = \frac{\beta_i^2 \Delta_i^2}{12} \end{aligned}$$

the third transition is based on changing the integration variable to $\tilde{t} = t - t_i$ and using the definition of t_i above. Since $\beta_i = \varphi'(t_i)$ the MSE of the i^{th} sampling interval becomes

$$MSE_i(a_{i-1}, a_i) \approx \frac{(\varphi'(t_i))^2 \Delta_i^2}{12}, \quad (9)$$

revealing the effect of signal-derivative energy on the sampling MSE.

Returning to the total sampling MSE, corresponding to optimal coefficients, and relying on its relation to the subintervals MSE yields (recall the implicit normalization to unit-interval length)

$$MSE\left(\{a_i\}_{i=1}^{N-1}\right) = \sum_{i=1}^N \Delta_i MSE_i(a_{i-1}, a_i) \quad (10)$$

$$= \frac{1}{12} \sum_{i=1}^N (\varphi'(t_i))^2 \Delta_i^3 \quad (11)$$

Let us connect our discussion to the prevalent approach of studying high-rate quantization based on the reproduction-value density function (see examples in [3], [13], [18], [19]). Following our scenario of high-resolution sampling we assume that the sampling-point layout can be described via a sampling-point density function, $\lambda(t)$, such that a small interval of length $\bar{\Delta}$ around \bar{t} approximately contains $\bar{\Delta} \cdot \lambda(\bar{t})$ sampling points. Moreover, the sampling-point density is related to the sampling intervals via

$$\lambda(t) \approx \frac{1}{N \cdot \Delta_i}, \quad \text{for } t \in [a_{i-1}, a_i]. \quad (12)$$

As we consider arbitrarily large values of N , the density $\lambda(t)$ is assumed to be a smoothly-varying continuous function.

Then, plugging the relation $\Delta_i \approx 1/(N \cdot \lambda(t_i))$ into the sampling-error expression (11), in addition to approximating the sum as an integral, yields

$$MSE(\lambda) = \frac{1}{12N^2} \int_0^1 \frac{(\varphi'(t))^2}{\lambda^2(t)} dt. \quad (13)$$

Here the sampling structure and the resulting MSE are determined by the sampling-point density $\lambda(t)$. The last MSE expression can be interpreted as the sampling equivalent of Bennett's integral for nonuniform quantization [1]. Commonly, the expression form in (13) is minimized via Hölder's inequality (see examples in [3], [18], [19]). For our problem, see details in the Appendix, we have the optimal sampling-point density given by

$$\lambda^{opt}(t) = \frac{\sqrt[3]{(\varphi'(t))^2}}{\int_0^1 \sqrt[3]{(\varphi'(z))^2} dz}, \quad (14)$$

and the optimal sampling MSE is

$$MSE(\lambda^{opt}) = \frac{1}{12N^2} \left(\int_0^1 \sqrt[3]{(\varphi'(t))^2} dt \right)^3. \quad (15)$$

The error expression in (15) is a product composed of two parts: sampling error for a simple linear signal (with a unit slope), and a term expressing the nonlinearity of the given signal based on its derivative energy. Moreover, Hölder's inequality also shows that (15) is the global minimum. The MSE expression in (15) is the sampling counterpart of the famous Panter-Dite formula for high-rate quantization MSE [2]. Evidently, while the quantization derivations were determined by the probability-density-function of the source, the sampling analysis provided here depends on the signal-derivative energy.

Using the sampling-point density, $\lambda(t)$, we can implement our nonuniform sampling via the companding design. Companding [1] is a widely-known technique for implementing nonuniform quantization based on a uniform quantizer. This is achieved by applying a nonlinear compressor function on the input value, then applying uniform quantization and mapping the result back via an expander function (the inverse of the compressor). Since in sampling we address the problem of discretizing the signal domain, the corresponding compressor and expander functions operate on the signal domain (i.e., as a nonlinear scaling of the time axis). The optimal compressor function is defined based on the optimal density (14) as

$$u(t) = \int_0^t \lambda^{opt}(z) dz = \frac{\int_0^t \sqrt[3]{(\varphi'(z))^2} dz}{\int_0^1 \sqrt[3]{(\varphi'(z))^2} dz}. \quad (16)$$

The corresponding expander, $v(\tau)$, is the inverse function of

the compressor, hence, it can be defined via the relation

$$\int_0^{v(\tau)} \lambda^{opt}(z) dz = \tau. \quad (17)$$

The last equation has a unique solution for strictly monotonic signals where the signal-derivative energy is positive over the entire domain, leading to a strictly-monotonic increasing compressor function (16) that is invertible and, thus, defines the expander function.

We suggest here a simple remedy for the case of non-monotonic signals. Since the problem occurs where the signal derivative is zero, we define the following extension of the derivative-energy:

$$g_\varepsilon^2(t) = \begin{cases} (\varphi'(t))^2 & \text{for } (\varphi'(t))^2 > \varepsilon \\ \varepsilon & \text{otherwise} \end{cases} \quad (18)$$

where $\varepsilon > 0$ is an arbitrarily small constant. The corresponding extension of the optimal sampling-point density is

$$\lambda_\varepsilon^{opt}(t) = \frac{\sqrt[3]{g_\varepsilon^2(t)}}{\int_0^1 \sqrt[3]{g_\varepsilon^2(z)} dz} \quad (19)$$

Accordingly, the density $\lambda_\varepsilon^{opt}(t)$ supports non-monotonic signals, while closely approximating the density $\lambda^{opt}(t)$ in (14). Replacing $\lambda^{opt}(t)$ with $\lambda_\varepsilon^{opt}(t)$ in (16)-(17) provides a practically useful compressor-expander pair.

While the expander function in (17) can be used as part of a companding architecture, we utilize it to construct the boundaries of the nonuniform segmentation via

$$a_i^{opt} = v\left(\frac{i}{N}\right) \quad , i = 1, \dots, N, \quad (20)$$

i.e., solving

$$\int_0^{a_i^{opt}} \lambda_\varepsilon^{opt}(z) dz = \frac{i}{N} \quad (21)$$

for $i = 1, \dots, N$.

B. Numerical Demonstrations

We now turn to study our theoretical results by applying them for analytic signals.

1) *Exponential Signals:* We consider an exponential signal of the form

$$\varphi(t) = e^{\alpha t} \quad , t \in [0, 1] \quad (22)$$

where $\alpha > 0$ is a real-valued parameter determining the growing rate (see examples in Fig. 1a). The signal-derivative energy is expressed as $(\varphi'(t))^2 = \alpha^2 e^{2\alpha t}$, which is positive valued for $t \in [0, 1]$ (Fig. 1b). Therefore, the optimal sampling-point density for this monotonic signal is expressed as

$$\lambda^{opt}(t) = \frac{2\alpha}{3} \cdot \frac{e^{\frac{2}{3}\alpha t}}{e^{\frac{2}{3}\alpha} - 1} \quad (23)$$

Plugging (23) into (17) defines the optimal expander, $v(\tau)$, via

$$\frac{e^{\frac{2}{3}\alpha v(\tau)} - 1}{e^{\frac{2}{3}\alpha} - 1} = \tau \quad (24)$$

that yields

$$v(\tau) = \frac{3}{2\alpha} \log \left(\left(e^{\frac{2}{3}\alpha} - 1 \right) \cdot \tau + 1 \right), \quad (25)$$

and the corresponding optimal nonuniform partitioning is determined via (20) as

$$a_i^{opt} = \frac{3}{2\alpha} \log \left(\left(e^{\frac{2}{3}\alpha} - 1 \right) \cdot \frac{i}{N} + 1 \right) \quad , i = 1, \dots, N \quad (26)$$

The MSE corresponding to the optimal nonuniform sampling is calculated using (15) and expressed as

$$MSE \left(\{a_i^{opt}\}_{i=1}^{N-1} \right) = \frac{9}{32\alpha N^2} \left(e^{\frac{2}{3}\alpha} - 1 \right)^3. \quad (27)$$

We evaluate the gain of our approach with respect to the uniform sampling. (for $i = 1, \dots, N$). The MSE of uniform high-resolution sampling is calculated by setting $a_i^{uniform} = \frac{i}{N}$ in the MSE expression in (11), yielding

$$MSE \left(\{a_i^{uniform}\}_{i=1}^{N-1} \right) = \frac{\alpha}{24N^2} (e^{2\alpha} - 1). \quad (28)$$

The MSE of the two sampling methods are compared in Fig. 1c and Fig. 1d for various exponential signals (via the α parameter) and sampling resolutions (the parameter N), respectively. Note that the MSE values are normalized by the signal energy, here expressed as $\int_{t=0}^1 \varphi^2(t) dt = \frac{1}{2\alpha} (e^{2\alpha} - 1)$. Figure 2 presents an example for the compressor function and the corresponding nonuniform sampling of an exponential signal.

2) *Cosine Signal:* Let us demonstrate our approach for a non-monotonic signal of the form:

$$\varphi(t) = \cos(2\pi\alpha t) \quad , t \in [0, 1] \quad (29)$$

where $\alpha > 0$ is an integer determining the number of periods contained in the $[0, 1]$ interval (see example for $\alpha = 5$ in Fig. 3a). The derivative energy of the cosine signal in (29) is

$$(\varphi'(t))^2 = 4\pi^2 \alpha^2 \sin^2(2\pi\alpha t) \quad , t \in [0, 1]. \quad (30)$$

As demonstrated in Fig. 3b, the signal-derivative energy is zero only at the points $t = \frac{j}{2\alpha}$ for $j = 0, 1, \dots, 2\alpha$. The compressor function does not lend itself here to a simple analytic form, nevertheless, it can be constructed numerically via its definition as a cumulative-density-function (see Eq. (16)) providing the compressor curve in Fig. 3c. The $2\alpha + 1$ points of zero signal-derivative energy are not a real obstacle in our numerical construction and, anyway, their corresponding values can be replaced by an arbitrarily small ε value¹ as suggested above. The expander function is numerically formed as the inverse of the compressor curve. The resulting nonuniform sampling structure (Fig. 3d) shows its adaptation to the local signal derivative and to the periodic nature of the signal.

¹In the numerical demonstrations provided here we set the value of ε to the smallest positive floating-point value available in Matlab via the command `eps`, which returns the value 2^{-52} .

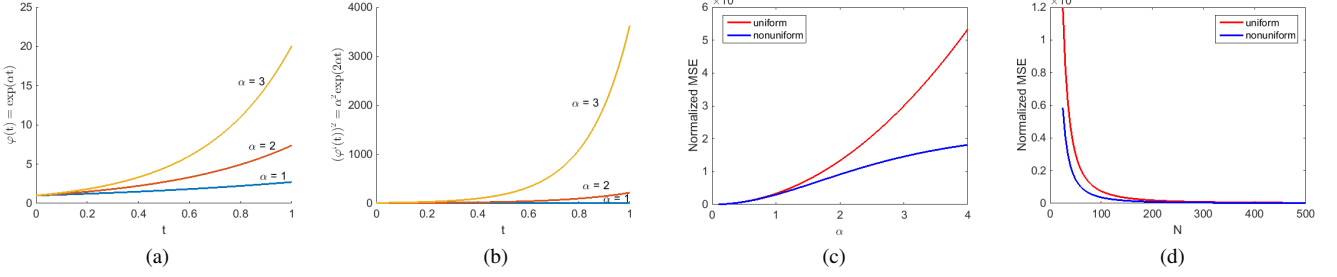


Fig. 1. Demonstration for an exponential signal $\varphi(t) = \exp(\alpha t)$ for $\alpha > 0$. (a) The exponential signal for several α values. (b) The signal-derivative energy for several α values. In (c)-(d), theoretical reconstruction-MSE obtained via nonuniform and uniform sampling procedures are compared. (c) evaluated for various α values and $N = 50$. (d) evaluated for a range of sampling resolutions (N) and $\alpha = 3$.

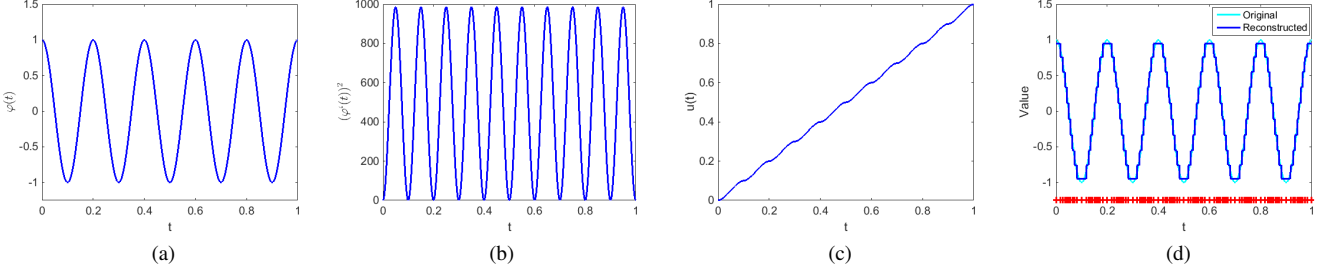


Fig. 3. Demonstration for a cosine signal $\varphi(t) = \cos(10\pi t)$. (a) The signal. (b) The signal-derivative energy. (c) The optimal compressor curve. (d) Optimal nonuniform sampling using $N = 100$ samples (the partitioning of the signal domain is in red).

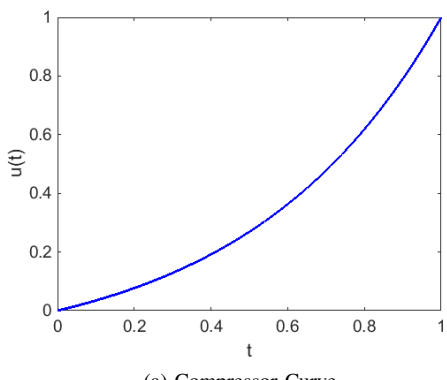


Fig. 2. Optimal nonuniform sampling ($N=50$) of an exponential signal $\varphi(t) = \exp(3t)$. (a) the mapping between uniform to nonuniform sampling-spacing. (b) shows the original signal (magenta), the reconstructed signal from nonuniform sampling (blue), and the partitioning to sampling intervals (red).

3) *Chirp Signal*: The cosine signal in (29) can be extended to the following chirp signal with a linearly increasing frequency:

$$\varphi(t) = \cos(2\pi t(1 + \alpha t)) \quad , \quad t \in [0, 1]. \quad (31)$$

Here the $\alpha > 0$ parameter determines the linear growth-rate of the frequency (Fig. 4a exemplifies this for $\alpha = 5$). The signal-derivative energy of the chirp (31) is

$$(\varphi'(t))^2 = 4\pi^2 (1 + 2\alpha t)^2 \sin^2(2\pi t(1 + \alpha t)) \quad , \quad t \in [0, 1]. \quad (32)$$

The nonuniform sampling of the chirp is demonstrated in Fig. 4d. Comparison between the nonuniform sampling of the cosine signal (Fig. 3) and the chirp signal (Fig. 4) reveals the influence of the varying frequency embodied in the chirp.

4) *Piecewise-Linear Signal*: Now we turn to evaluate our sampling method on a piecewise-linear signal containing a significant portion of a constant value. This will show the suitability of the proposed method also to signals with a zero derivative-energy over a large continuous sub-interval. We define here a specific signal form as

$$\varphi(t) = \begin{cases} 5t & \text{for } t \in [0, \alpha) \\ (t - \alpha) + 5\alpha & \text{for } t \in [\alpha, 2\alpha) \\ 6\alpha & \text{for } t \in [2\alpha, 1 - 2\alpha) \\ -(t - (1 - 2\alpha)) + 6\alpha & \text{for } t \in [1 - 2\alpha, 1 - \alpha) \\ -5(t - (1 - \alpha)) + 5\alpha & \text{for } t \in [1 - \alpha, 1] \end{cases} \quad (33)$$

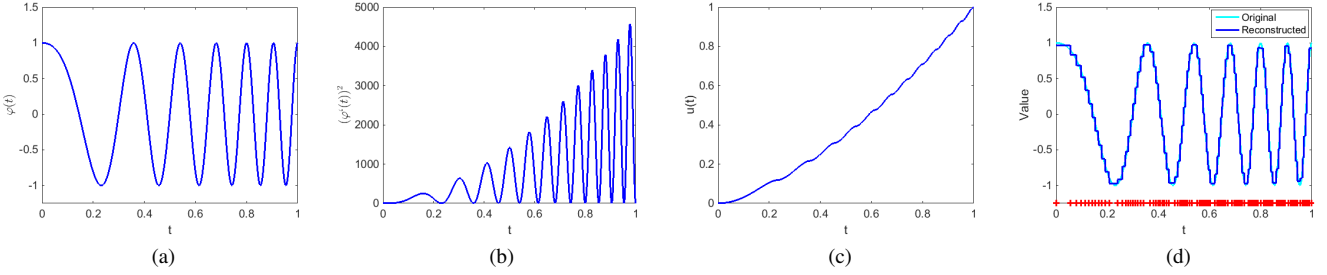


Fig. 4. Demonstration for a chirp signal $\varphi(t) = \cos(2\pi t(1+5t))$. (a) The signal. (b) The signal-derivative energy. (c) The optimal compressor curve. (d) Optimal nonuniform sampling using $N = 100$ samples (the partitioning of the signal domain is in red).

and the corresponding signal-derivative energy is

$$(\varphi'(t))^2 = \begin{cases} 25 & \text{for } t \in [0, \alpha) \cup [1 - \alpha, 1] \\ 1 & \text{for } t \in [\alpha, 2\alpha) \cup [1 - 2\alpha, 1 - \alpha] \\ 0 & \text{for } t \in [2\alpha, 1 - 2\alpha]. \end{cases} \quad (34)$$

Figure 5 demonstrates the sampling procedure for a piecewise-linear signal constructed for $\alpha = \frac{1}{8}$. Fig. 5d shows that using the extended sampling-point density function from (19), where small derivative-energy values are clipped to ε , provides a good solution to the constant-valued region of this signal.

III. EXPERIMENTAL RESULTS: SAMPLING OF ONE-DIMENSIONAL SIGNALS

In this section we present experimental evaluations of the procedure proposed in section II for nonuniform sampling of one-dimensional signals.

A. The Main Competing Method: Tree-Structured Nonuniform Sampling

Let us consider sampling based on a nonuniform partitioning that is represented using a binary tree. The approach examined here is inspired by the general framework given in [20] for optimizing tree-structures for various tasks, and is also influenced by the discrete Lagrangian optimization approach [21] and its application in coding [22], [23].

The suggested approach relies on an initial tree, which is a full d -depth binary-tree, representing a uniform segmentation of the interval $[0, 1]$ into 2^d sampling intervals of 2^{-d} length (see example in Fig. 6a). The segmentation of the interval $[0, 1]$ is described by the leaves of the binary tree: the interval location and length are defined by the leaf position in the tree, specifically, the tree-level where the leaf resides in determines the interval length. The examined nonuniform segmentations are induced by all the trees obtained by repeatedly pruning neighboring-leaves having the same parent node (examples are given in Figures 6b-6c). The initial d -depth full-tree together with all its pruned subtrees form the set of relevant trees, denoted here as \mathcal{T}_d .

The leaves of a tree $T \in \mathcal{T}_d$ form a set denoted as $L(T)$, where the number of leaves is referred to as $|L(T)|$. Accordingly, the tree T represents a (possibly) nonuniform

partitioning of the $[0, 1]$ interval into $|L(T)|$ sampling intervals. A leaf $l \in L(T)$ resides in the $h(l)$ level of the tree and corresponds to the interval $[a_{(l)}^{left}, a_{(l)}^{right}]$ of length $\Delta(l) = 2^{-h(l)}$. Following the analysis in section II, the optimal sample corresponding to the leaf $l \in L(T)$ is expressed via (4) as

$$\varphi_{(l)}^{opt} = \frac{1}{\Delta(l)} \int_{a_{(l)}^{left}}^{a_{(l)}^{right}} \varphi(t) dt. \quad (35)$$

Consequently, as the tree leaves correspond to a segmentation of the $[0, 1]$ interval, the sampling MSE induced by the tree $T \in \mathcal{T}_d$ is calculated based on the leaves, $L(T)$, via

$$MSE(T) = \sum_{l \in L(T)} \int_{a_{(l)}^{left}}^{a_{(l)}^{right}} (\varphi(t) - \varphi_{(l)}^{opt})^2 dt. \quad (36)$$

For a signal $\varphi(t)$ and a budget of N samples, one can formulate the optimization of a tree-structured nonuniform sampling as

$$\begin{aligned} & \underset{T \in \mathcal{T}_d}{\text{minimize}} \quad MSE(T) \\ & \text{subject to} \quad |L(T)| = N, \end{aligned} \quad (37)$$

i.e., the optimization searches for the tree with N leaves that provides minimal sampling MSE. The unconstrained Lagrangian form of (37) is

$$\min_{T \in \mathcal{T}_d} MSE(T) + \mu |L(T)|, \quad (38)$$

where $\mu \geq 0$ is a Lagrange multiplier that reflects the constraint $|L(T)| = N$. However, it should be noted that due to the discrete nature of the problem such μ does not necessarily exist for any N value (for details see, e.g., [20], [21]). The problem (38) can also be written as

$$\min_{T \in \mathcal{T}_d} \sum_{l \in L(T)} \int_{a_{(l)}^{left}}^{a_{(l)}^{right}} (\varphi(t) - \varphi_{(l)}^{opt})^2 dt + \mu |L(T)|. \quad (39)$$

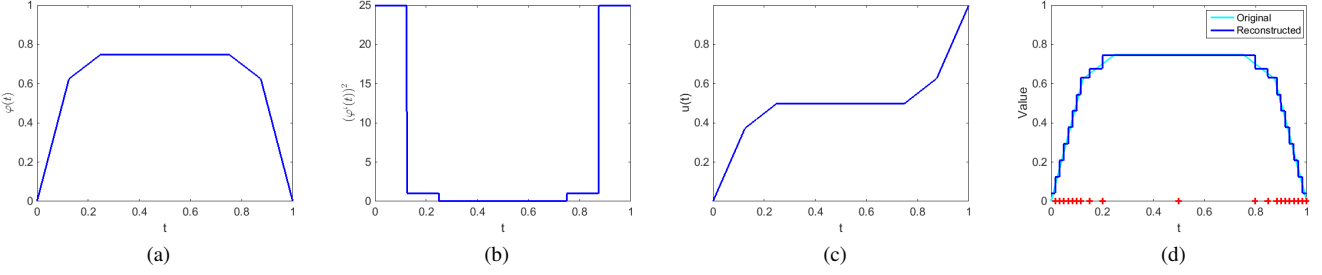


Fig. 5. Demonstration for a piecewise-linear signal as in Eq. (33) with $\alpha = \frac{1}{8}$. (a) The signal. (b) The signal-derivative energy. (c) The optimal compressor curve. (d) Optimal nonuniform sampling via the extended sampling-point density using $N = 20$ samples (the partitioning of the signal domain is in red).

Note that, due to the non-intersecting sampling intervals, a leaf $l \in L(T)$ contributes the Lagrangian cost

$$C(l) = \int_{a_{(l)}^{left}}^{a_{(l)}^{right}} \left(\varphi(t) - \varphi_{(l)}^{opt} \right)^2 dt + \mu, \quad (40)$$

corresponding to a single sampling interval.

The discrete optimization problem (39) of finding the optimal tree for a given signal and a Lagrange multiplier μ is addressed by the following procedure. Start from the full d -depth tree and determine the corresponding sampling intervals and their optimal samples, squared errors, and Lagrangian costs (40). Go through the tree levels from bottom and up, in each tree level find the pairs of neighboring leaves having the same parent node and evaluate the pruning condition: if

$$C(\text{left child}) + C(\text{right child}) > C(\text{parent}) \quad (41)$$

is true, then prune the two leaves – implying that two sampling intervals are merged to form a single interval of double length (thus, the total samples in the partitioning is reduced by one). If the condition (41) is false, then the two leaves (and the corresponding sampling intervals) are kept. This procedure is continued until reaching a level where no pruning is done, or when getting to the tree root.

B. Evaluation and Comparison

The proposed sampling method is compared to two other sampling approaches. The first is the trivial, however commonly-used, uniform sampling, where the signal domain is partitioned into equal-size sampling-intervals. Specifically, for a budget of N samples the signal domain $[0, 1]$ is segmented according to $a_i = \frac{i}{N}$ for $i = 0, 1, \dots, N$. The samples are determined as the averages of the corresponding sampling intervals. The second competing method is a nonuniform sampling based on a binary-tree structure that is adapted to the signal via a Lagrange optimization, as presented in the previous subsection.

We examined sampling of several signals defined analytically. A grid of μ values was set for the tree-structured Lagrange optimization, this determined the number of sam-

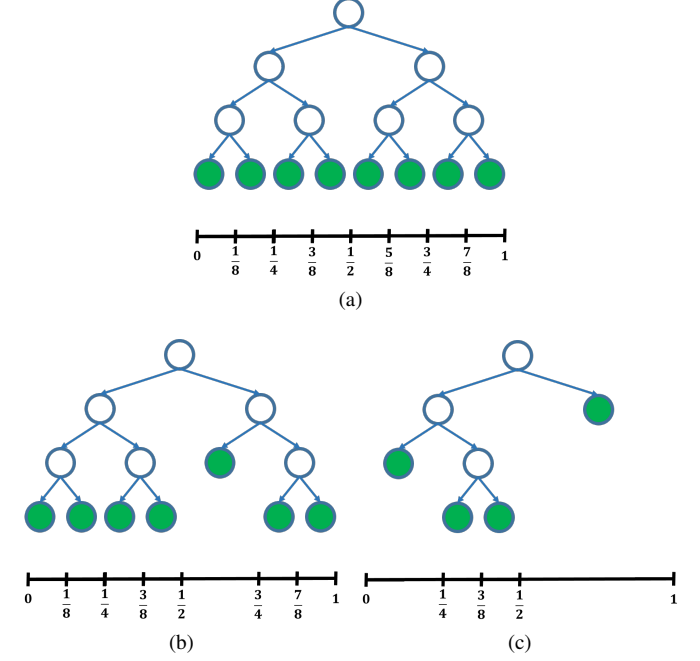


Fig. 6. Segmentations of the $[0, 1]$ interval produced by binary trees. The leaves, which determine the partitioning, are colored in green. (a) A full binary tree of depth 3 and the corresponding uniform segmentation into 8 sub-intervals. (b) A tree obtained by a single pruning of the full tree, thus the partitioning includes 7 sub-intervals. (c) A tree obtained by several prunings resulting in 4 leaves/segments.

ples to consider². First, the sampling of the cosine signal $\varphi(t) = 255 \cdot \cos(10\pi t)$ was examined, and showed that our method consistently outperforms the uniform and the tree-structured techniques for various amounts of samples (Fig. 7a). These observations were further established by examining sampling of the chirp signal, $\varphi(t) = 255 \cdot \cos(2\pi t(1+5t))$, and the piecewise-linear signal from Eq. (33) that was scaled by a factor of 255 (Figures 7b-7c).

IV. ANALYSIS FOR MULTIDIMENSIONAL SIGNALS

In this section we discuss the theoretic analysis of optimal high-resolution sampling by studying the problem for

²Note that the proposed method and the uniform sampling do not rely on μ and operate directly based on a given number of samples, however, we defined the examined sample budgets based on the μ grid of the tree-structured sampling in order to maintain an accurate comparison between all the sampling methods.

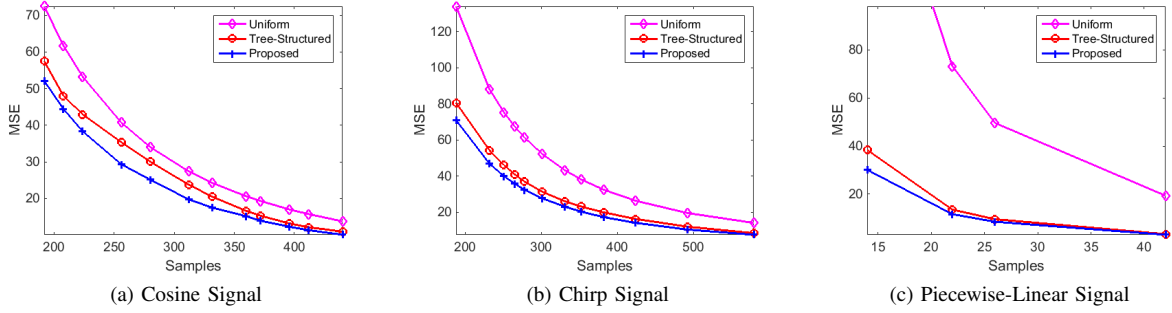


Fig. 7. Performance comparison of the proposed sampling method, the uniform sampling approach, and optimized tree-structured sampling. The curves present the sampling MSE obtained for various sample budgets.

sampling multidimensional signals. The analysis for the one-dimensional case is relatively simple since the partition is characterized by sampling-interval lengths (see section II). However, when considering the multidimensional problem the required analysis becomes more intricate as the sampling regions are, in general, of arbitrary shape and size. Accordingly, our analysis in this section is conceptually and mathematically similar to the study of multidimensional high-rate quantization provided by Gersho [3], which generalized the one-dimensional theory of Bennett [1] and the distortion formula of Panter and Dite [2]. Thus, we provide a theoretic framework for optimal multidimensional signal sampling at high resolution.

The given signal, $\varphi(\mathbf{x})$, is defined over a K -dimensional unit cube, $\mathcal{C}^K \triangleq [0, 1]^K$, and is scalar real-valued from a bounded range, i.e., $\varphi(\mathbf{x}) \in [\varphi_L, \varphi_H]$ for any $\mathbf{x} \in \mathcal{C}^K$. The signal goes through a sampling procedure in order to provide a discrete representation using $N \in \mathbb{N}$ (scalar valued) samples, $\{\varphi_i\}_{i=1}^N$, corresponding to a partitioning of \mathcal{C}^K to N distinct multidimensional regions, $\{A_i\}_{i=1}^N$, such that $\bigcup_{i=1}^N A_i = \mathcal{C}^K$. Again, we consider a reconstruction procedure providing the continuous-domain piecewise-constant signal

$$\hat{\varphi}(\mathbf{x}) = \varphi_i \quad \text{for } \mathbf{x} \in A_i, \quad (42)$$

and optimization in the sense of minimizing the overall MSE, here formulated as (note the implicit normalization in the unit-cube volume)

$$MSE\left(\{A_i\}_{i=1}^N, \{\varphi_i\}_{i=1}^N\right) = \sum_{i=1}^N \int_{A_i} (\varphi(\mathbf{x}) - \varphi_i)^2 d\mathbf{x}. \quad (43)$$

Moreover, as before, the optimal sampling coefficients given the partitioning $\{A_i\}_{i=1}^N$ can be analytically determined, showing that

$$\varphi_i^{opt} = \frac{1}{V(A_i)} \int_{A_i} \varphi(\mathbf{x}) d\mathbf{x}, \quad i = 1, \dots, N \quad (44)$$

where $V(A_i)$ is the volume of the region A_i .

We consider the case of optimal high-resolution sampling (i.e., N is very large), and assume that the optimal sampling regions are all small enough and appropriately shaped such that we can further presume that the signal $\varphi(\mathbf{x})$ is well

approximated within each region by a linear form that is locally determined. More specifically,

$$\varphi(\mathbf{x}) \approx \beta_i^T \mathbf{x} + \gamma_i \quad \text{for } \mathbf{x} \in A_i, \quad (45)$$

where β_i is a K -dimensional column vector and γ_i is a scalar value. Moreover, the above linear form can be determined in the i^{th} region by the first-order Taylor approximation of the signal around the region center, $\mathbf{x}_i \triangleq \frac{1}{V(A_i)} \int_{A_i} \mathbf{x} d\mathbf{x}$, namely,

$$\varphi(\mathbf{x}) \approx \varphi(\mathbf{x}_i) + \nabla \varphi(\mathbf{x}_i) (\mathbf{x} - \mathbf{x}_i) \quad (46)$$

where $\nabla \varphi(\mathbf{x}_i)$ is the signal gradient, evaluated at the region center, here having the form of a K -length row vector consisting of the K partial derivatives, i.e.,

$$\nabla \varphi(\mathbf{x}_i) = \left[\frac{\partial \varphi(\mathbf{x})}{\partial x_1} \Big|_{\mathbf{x}=\mathbf{x}_i}, \frac{\partial \varphi(\mathbf{x})}{\partial x_2} \Big|_{\mathbf{x}=\mathbf{x}_i}, \dots, \frac{\partial \varphi(\mathbf{x})}{\partial x_K} \Big|_{\mathbf{x}=\mathbf{x}_i} \right], \quad (47)$$

where $\frac{\partial \varphi(\mathbf{x})}{\partial x_j} \Big|_{\mathbf{x}=\mathbf{x}_i}$ is the partial derivative of the signal in the j^{th} standard direction ($j = 1, \dots, K$) measured at the region central point \mathbf{x}_i . Accordingly, the linear-form parameters of the i^{th} region are set to

$$\beta_i^T = \nabla \varphi(\mathbf{x}_i) \quad (48)$$

$$\gamma_i = \varphi(\mathbf{x}_i) - \nabla \varphi(\mathbf{x}_i) \mathbf{x}_i. \quad (49)$$

The local linear approximation within each region (45) yields an optimal sampling coefficient that is approximately the signal value at the region center, i.e.,

$$\varphi_i^{opt} \approx \frac{1}{V(A_i)} \int_{A_i} (\beta_i^T \mathbf{x} + \gamma_i) d\mathbf{x} = \beta_i^T \mathbf{x}_i + \gamma_i \approx \varphi(\mathbf{x}_i). \quad (50)$$

Then, the sampling MSE of the i^{th} region is

$$\begin{aligned} MSE_i(A_i) &= \frac{1}{V(A_i)} \int_{A_i} (\varphi(\mathbf{x}) - \varphi_i^{opt})^2 d\mathbf{x} \\ &\approx \frac{1}{V(A_i)} \int_{A_i} [\beta_i^T \mathbf{x} + \gamma_i - (\beta_i^T \mathbf{x}_i + \gamma_i)]^2 d\mathbf{x} \\ &= \frac{1}{V(A_i)} \|\beta_i\|_2^2 \int_{A_i} \|\mathbf{x} - \mathbf{x}_i\|_2^2 d\mathbf{x}. \end{aligned} \quad (51)$$

Inspired by the analysis given by Gersho [3] to high-rate quantization, we turn to interpret the last error expression using the normalized moment of inertia of the region A_i around its center \mathbf{x}_i , defined as

$$M(A_i) \triangleq \frac{\int_{A_i} \|\mathbf{x} - \mathbf{x}_i\|_2^2 d\mathbf{x}}{K \cdot V(A_i)^{1+\frac{2}{K}}}, \quad (52)$$

where this quantity is invariant to proportional scaling of the region. Now the region MSE becomes

$$MSE_i(A_i) = K \|\beta_i\|_2^2 M(A_i) V(A_i)^{\frac{2}{K}}, \quad (53)$$

and the total MSE is expressed as

$$\begin{aligned} MSE\left(\{A_i\}_{i=1}^N\right) &= \sum_{i=1}^N V(A_i) \cdot MSE_i(A_i) \\ &= K \sum_{i=1}^N \|\beta_i\|_2^2 M(A_i) V(A_i)^{1+\frac{2}{K}}. \end{aligned} \quad (54)$$

We now assume that in the high-resolution scenario there is a sampling-point density function, $\lambda(\mathbf{x})$, such that for any small volume A that contains \mathbf{x} , the fraction of sampling points contained in it is approximately $\lambda(\mathbf{x}) V(A)$. Furthermore, the density function satisfies the approximate relation

$$\lambda(\mathbf{x}) \approx \frac{1}{N \cdot V(A_i)}, \quad \text{for } \mathbf{x} \in A_i. \quad (55)$$

Hence, the above assumption implies that adjacent sampling regions have similar density values.

Na and Neuhoff [19] introduced (in the context of vector quantization) the important notion of the inertial profile, denoted here as $m(\mathbf{x})$. The function $m(\mathbf{x})$ is assumed to be smooth and to approximate the normalized moment of inertia of the cells (around their mass centers) in the neighborhood of \mathbf{x} . The smoothness of the inertial profile is based on the assumption that neighboring regions have similar values of normalized moment of inertia in a high-resolution segmentation.

The definitions of the sampling-point density function in (55) and the inertial profile let us to express the MSE in (54) as

$$MSE\left(\{A_i\}_{i=1}^N\right) = \frac{K}{N^{\frac{2}{K}}} \sum_{i=1}^N \|\beta_i\|_2^2 \frac{m(\mathbf{x}_i)}{\lambda(\mathbf{x}_i)^{\frac{2}{K}}} V(A_i). \quad (56)$$

Furthermore, due to the high-resolution assumption we approximate the previous sum by the following integral,

$$MSE(\lambda, m) = \frac{K}{N^{\frac{2}{K}}} \int_{\mathcal{C}^K} \beta^2(\mathbf{x}) \frac{m(\mathbf{x})}{\lambda(\mathbf{x})^{\frac{2}{K}}} d\mathbf{x}. \quad (57)$$

where

$$\beta^2(\mathbf{x}) \triangleq \|\nabla \varphi_{(\mathbf{x})}\|_2^2. \quad (58)$$

The error expression in (57) can be interpreted as Bennett's integral for multidimensional sampling. This formula shows that the sampling MSE for a given signal, which is represented

by its gradient-energy density, is determined by the sampling point density and the inertial profile of the sampling structure.

We now argue that optimal high-resolution sampling of a multidimensional linear signal with a uniform gradient-energy density evaluated as 1 everywhere in \mathcal{C}^K is obtained by partitioning the signal domain, \mathcal{C}^K , based on a tessellation generated by a single optimal (in the sense of minimum normalized moment of inertia) convex polytope, A_K^* , such that all the regions in the segmentation are congruent to it³. Accordingly, this optimal division results in a constant normalized moment of inertia to all of the sampling regions, namely,

$$M(A_i) = M(A_K^*) \quad \text{for } i = 1, \dots, N, \quad (59)$$

or in inertial profile terms: $m(\mathbf{x}) = M(A_K^*)$, i.e., a constant function. We further assume that optimal high-resolution sampling of a nonlinear signal is obtained by regions that are approximately congruent and scaled versions of the optimal polytope used for sampling a linear signal. Then, Eq. (59) is satisfied also in our case of sampling a nonlinear signal, since scaling does not change the normalized moment of inertia. The latter hypothesis mirrors the conjecture made by Gersho in [3] for high-rate quantization. Consequently, the MSE expression (57) is reformed to

$$MSE(\lambda) = \frac{K \cdot M(A_K^*)}{N^{\frac{2}{K}}} \int_{\mathbf{x} \in \mathcal{C}^K} \beta^2(\mathbf{x}) \frac{1}{\lambda(\mathbf{x})^{\frac{2}{K}}} d\mathbf{x}. \quad (60)$$

We optimize the sampling procedure by characterizing the best sampling-point density, $\lambda^{opt}(\mathbf{x})$, that minimizes the MSE as expressed in (60). Similar to the optimization in the one-dimensional case (see the Appendix), we rely on Hölder's inequality that provides us a lower bound to the MSE in (60) in the form of

$$MSE(\lambda) \geq \frac{K \cdot M(A_K^*)}{N^{\frac{2}{K}}} \left(\int_{\mathbf{x} \in \mathcal{C}^K} (\beta^2(\mathbf{x}))^{\frac{K}{K+2}} d\mathbf{x} \right)^{1+\frac{2}{K}} \quad (61)$$

Here, following the application of Hölder's inequality, the MSE lower bound is attained when $\lambda(\mathbf{x})$ is proportional to $\beta^2(\mathbf{x})^{\frac{1}{(\lambda(\mathbf{x}))^{\frac{2}{K}}}}$ implying that the optimal sampling point density is

$$\lambda^{opt}(\mathbf{x}) = \frac{(\beta^2(\mathbf{x}))^{\frac{K}{K+2}}}{\int_{\mathbf{z} \in \mathcal{C}^K} (\beta^2(\mathbf{z}))^{\frac{K}{K+2}} d\mathbf{z}}. \quad (62)$$

Note that we used the fact that integrating a density function over the entire domain should be 1.

The optimal sampling-point density demonstrates that in regions where the derivative energy is higher, the sampling should be denser by reducing the volumes of the relevant sampling regions. Moreover, returning to the discrete formulation

³Based on the high-resolution assumption, we neglect cells that are intersected by the boundary of the signal domain, \mathcal{C}^K , and thus may not be congruent to the optimal tessellating polytope.

for high-resolution sampling MSE in (54) and by utilizing (55) together with (62) and (59) shows that in the optimal solution all the sampling regions contribute the same amount of MSE. In addition, the results in this section are generalization of those obtained in the analysis of one-dimensional signals in the previous section, this can be observed by setting $K = 1$ and $M(A_1^*) = \frac{1}{12}$, which is the normalized moment of inertia for one-dimensional intervals (or any other K -dimensional cube) around their center.

The high-resolution analysis provides a theoretic evaluation of a sampler based on its sampling-point density function. As we described above, the suggested framework lets to determine the optimal sampling procedure in terms of the best sampling-point density function. In the one-dimensional case the sampling-point density can be directly translated to a practical sampling procedure via the companding model (see sections II and III-B). However, in the multidimensional case, in general, there are no direct ways to implement a sampler based on a given sampling-point density function. This conclusion is based on the following results from the quantization field [3], [24], [25]. In [24], [25] it was shown that optimal companding requires a compressor function that is a conformal mapping. This result implies that a direct implementation of multidimensional sampler based on a given point density is limited to a minor class of signals with a suitable gradient-energy density – thus, in general, optimal multidimensional companding is impractical. This result was followed by a treatment of multidimensional companding for the vector quantization problem in limited settings that consider suboptimal solutions and/or particular source distributions [26]–[29]. Consequently, as in the high-rate quantization literature, the analysis provided here for the multidimensional case is a theoretic framework for studying sampling of multidimensional signals. Specifically, it describes the optimal sampler and allows to assess its theoretic performance. This together with Bennett's integral for multidimensional sampling (Eq. (57)) can be used to evaluate the performance of practical suboptimal sampling procedures (similar to the analysis of practical vector quantizers in [19]).

V. CONCLUSION

We analyze the topic of nonuniform sampling of deterministic signals as a mirror-image of nonuniform quantization. With the advent of new technologies, adaptive sampling becomes a viable alternative to be considered in data compression applications. In all the above developments, the crucial local-density controlling parameter turns out to be the local energy of the signal gradient. A new adaptive sampling method for one-dimensional signals is proposed and experimentally established as a leading nonuniform-sampling approach.

APPENDIX

SAMPLING-POINT DENSITY OPTIMIZATION VIA HÖLDER'S INEQUALITY FOR THE ONE-DIMENSIONAL CASE

We aim at minimizing the sampling MSE given in (13) as

$$MSE(\lambda) = \frac{1}{12N^2} \int_0^1 \frac{(\varphi'(t))^2}{\lambda^2(t)} dt. \quad (63)$$

Using Hölder's inequality we can write

$$\begin{aligned} \left(\int_0^1 \left(\sqrt[3]{(\varphi'(t))^2} \cdot \frac{1}{\lambda^{\frac{2}{3}}(t)} \right)^3 dt \right)^{\frac{1}{3}} &\left(\int_0^1 \left(\lambda^{\frac{2}{3}}(t) \right)^{\frac{3}{2}} dt \right)^{\frac{2}{3}} \\ &\geq \int_0^1 \sqrt[3]{(\varphi'(t))^2} dt. \end{aligned} \quad (64)$$

Simplifying the left side of (64) gives

$$\begin{aligned} \left(\int_0^1 (\varphi'(t))^2 \cdot \frac{1}{\lambda^2(t)} dt \right)^{\frac{1}{3}} &\left(\int_0^1 \lambda(t) dt \right)^{\frac{2}{3}} \\ &\geq \int_0^1 \sqrt[3]{(\varphi'(t))^2} dt. \end{aligned} \quad (65)$$

Then, since $\lambda(t)$ is a density function its integration over the entire domain equals to 1, reducing (65) into

$$\int_0^1 (\varphi'(t))^2 \cdot \frac{1}{\lambda^2(t)} dt \geq \left(\int_0^1 \sqrt[3]{(\varphi'(t))^2} dt \right)^3. \quad (66)$$

Here, Hölder's inequality is attained with equality when $\lambda(t)$ is proportional to $(\varphi'(t))^2 \cdot \frac{1}{\lambda^2(t)}$, therefore, the optimal sampling-point density is

$$\lambda^{opt}(t) = \frac{\sqrt[3]{(\varphi'(t))^2}}{\int_0^1 \sqrt[3]{(\varphi'(z))^2} dz}. \quad (67)$$

Setting the lower bound from (66), which is achieved by $\lambda^{opt}(t)$, in the MSE expression from (63) gives the following optimal sampling MSE

$$MSE(\lambda^{opt}) = \frac{1}{12N^2} \left(\int_0^1 \sqrt[3]{(\varphi'(t))^2} dt \right)^3. \quad (68)$$

REFERENCES

- [1] W. R. Bennett, "Spectra of quantized signals," *Bell System Technical Journal*, vol. 27, no. 3, pp. 446–472, 1948.
- [2] P. Panter and W. Dite, "Quantization distortion in pulse-count modulation with nonuniform spacing of levels," *Proceedings of the IRE*, vol. 39, no. 1, pp. 44–48, 1951.
- [3] A. Gersho, "Asymptotically optimal block quantization," *IEEE Transactions on information theory*, vol. 25, no. 4, pp. 373–380, 1979.
- [4] E. Shusterman and M. Feder, "Image compression via improved quadtree decomposition algorithms," *IEEE Transactions on Image Processing*, vol. 3, no. 2, pp. 207–215, 1994.
- [5] R. Shukla, P. L. Dragotti, M. N. Do, and M. Vetterli, "Rate-distortion optimized tree-structured compression algorithms for piecewise polynomial images," *IEEE Transactions on Image Processing*, vol. 14, no. 3, pp. 343–359, 2005.
- [6] R. A. Ulichney, "Review of halftoning techniques," in *Electronic Imaging*, 1999, pp. 378–391.
- [7] D. L. Lau and R. Ulichney, "Blue-noise halftoning for hexagonal grids," *IEEE Transactions on Image Processing*, vol. 15, no. 5, pp. 1270–1284, 2006.
- [8] D. P. Mitchell, "Generating antialiased images at low sampling densities," in *ACM SIGGRAPH Computer Graphics*, vol. 21, no. 4, 1987, pp. 65–72.

- [9] ——, “Spectrally optimal sampling for distribution ray tracing,” in *ACM SIGGRAPH Computer Graphics*, vol. 25, no. 4, 1991, pp. 157–164.
- [10] M. McCool and E. Fiume, “Hierarchical poisson disk sampling distributions,” in *Proceedings of the Conference on Graphics Interface*, vol. 92, 1992, pp. 94–105.
- [11] R. Fattal, “Blue-noise point sampling using kernel density model,” in *ACM Transactions on Graphics (TOG)*, vol. 30, no. 4, 2011, p. 48.
- [12] Z. Zhong and J. Hua, “Kernel-based adaptive sampling for image reconstruction and meshing,” *Computer Aided Geometric Design*, vol. 43, pp. 68–81, 2016.
- [13] S. Lloyd, “Least squares quantization in PCM,” *IEEE Transactions on Information Theory*, vol. 28, no. 2, pp. 129–137, 1982.
- [14] D. Newman, “The hexagon theorem,” *IEEE Transactions on Information Theory*, vol. 28, no. 2, pp. 137–139, 1982.
- [15] E. Barnes and N. Sloane, “The optimal lattice quantizer in three dimensions,” *SIAM Journal on Algebraic Discrete Methods*, vol. 4, no. 1, pp. 30–41, 1983.
- [16] Q. Du and D. Wang, “The optimal centroidal voronoi tessellations and the gersho’s conjecture in the three-dimensional space,” *Computers & Mathematics with Applications*, vol. 49, no. 9, pp. 1355–1373, 2005.
- [17] P. Zador, “Asymptotic quantization error of continuous signals and the quantization dimension,” *IEEE Transactions on Information Theory*, vol. 28, no. 2, pp. 139–149, 1982.
- [18] R. M. Gray and D. L. Neuhoff, “Quantization,” *IEEE Transactions on Information Theory*, vol. 44, no. 6, pp. 2325–2383, 1998.
- [19] S. Na and D. L. Neuhoff, “Bennett’s integral for vector quantizers,” *IEEE Transactions on Information Theory*, vol. 41, no. 4, pp. 886–900, 1995.
- [20] P. A. Chou, T. Lookabaugh, and R. M. Gray, “Optimal pruning with applications to tree-structured source coding and modeling,” *IEEE Transactions on Information Theory*, vol. 35, no. 2, pp. 299–315, 1989.
- [21] H. Everett III, “Generalized lagrange multiplier method for solving problems of optimum allocation of resources,” *Operations Research*, vol. 11, no. 3, pp. 399–417, 1963.
- [22] Y. Shoham and A. Gersho, “Efficient bit allocation for an arbitrary set of quantizers,” *IEEE Transactions on Acoustics, Speech, and Signal Processing*, vol. 36, no. 9, pp. 1445–1453, 1988.
- [23] A. Ortega and K. Ramchandran, “Rate-distortion methods for image and video compression,” *IEEE Signal Processing Magazine*, vol. 15, no. 6, pp. 23–50, 1998.
- [24] J. Bucklew, “Companding and random quantization in several dimensions,” *IEEE Transactions on Information Theory*, vol. 27, no. 2, pp. 207–211, 1981.
- [25] ——, “A note on optimal multidimensional companders (corresp.),” *IEEE Transactions on Information Theory*, vol. 29, no. 2, pp. 279–279, 1983.
- [26] P. Moo and D. Neuhoff, “Optimal compressor functions for multidimensional companding,” in *IEEE International Symposium on Information Theory*, 1997, p. 515.
- [27] S. F. Simon, “On suboptimal multidimensional companding,” in *Data Compression Conference, 1998. DCC’98. Proceedings*, 1998, pp. 438–447.
- [28] J. Samuelsson, “Multidimensional companding quantization of the gaussian source,” *IEEE Transactions on Information Theory*, vol. 49, no. 5, pp. 1343–1351, 2003.
- [29] Z. H. Perić, O. D. Milanović, and A. Ž. Jovanović, “Optimal companding vector quantization for circularly symmetric sources,” *Information Sciences*, vol. 178, no. 22, pp. 4375–4381, 2008.